Structural Phase Transition of Magnetic $[Ni(dmit)_2]^-$ Salts Induced by Supramolecular Cation Structures of $(M^+)([12]crown\text{-}4)_2$

Tomoyuki Akutagawa,*,†,‡,§ Takeshi Motokizawa,‡ Kazumasa Matsuura,‡ Sadafumi Nishihara,‡ Shin-ichiro Noro,†,‡ and Takayoshi Nakamura*,†,‡,§

Research Institute for Electronic Science, Hokkaido University, Sapporo 060-0812, Japan, Graduate School of Environmental Earth Science, Hokkaido University, Sapporo 060-0810, Japan, and CREST, Japan Science and Technology Agency (JST), Kawaguchi 332-0012, Japan

Received: September 30, 2005; In Final Form: January 18, 2006

Sandwich-type supramolecular cation structures of $(M^+)([12]crown\text{-}4)_2$ complexes ($M^+ = Li^+$, Na^+, K^+, and Rb^+) were introduced as countercations to the $[Ni(dmit)_2]^-$ anion, which bears an $S = {}^1/_2$ spin, to form novel magnetic crystals ($dmit^{2-}$ = 2-thione-1,3-dithiole-4,5-dithiolate). The zigzag arrangement of $Li^+([12]crown\text{-}4)_2$ cations in $Li^+([12]crown\text{-}4)_2[Ni(dmit)_2]^-$ salt induced weak intermolecular interactions of $[Ni(dmit)_2]^-$ dimers, whose magnetic spins were isolated from each other. The molecular arrangements of cations and anions in $M^+([12]crown\text{-}4)_2[Ni(dmit)_2]^-$ salts ($M^+ = Na^+$, K^+, and Rb^+) were isostructural to each other. In the case of $Na^+([12]crown\text{-}4)_2[Ni(dmit)_2]^-$, the space group *C*2/*m* changed to *C*2/c with a lowering in temperature from 298 to 100 K. This structural change occurred at 222.5 K as a first-order phase transition. The space group *C*2/*m* ($T = 298$ K) in the salt $K^+([12]crown\text{-}4)_2[Ni(dmit)_2]^-$ also changed to *C*2/*c* ($T = 100$ K), which transition occurred at 270 K. Crystal structural analyses at 298 and 100 K revealed changes in both supramolecular cation conformation and $[Ni(dmit)_2]^-$ anion arrangements. The transition from *C*2/*m* to *C*2/*c* crystals generated a dipole moment in the $Na^+([12]crown\text{-}4)_2$ and $K^+([12]crown\text{-}4)_2$ structures, which were reconstructed to cancel the net dipole moment of the *C*2/*c* crystals. These cation transformations led to changes in intermolecular interactions between the $[Ni(dmit)_2]^-$ anions via structural rearrangements. The crystal structure of *C*2/*c* was stabilized in $Rb^+([12]crown\text{-}4)_2[Ni(dmit)_2]^-$ at 298 K. The $[Ni(dmit)_2]^-$ configuration in these salts with the *C*2/*c* space group was a one-dimensional uniform chain, which showed the temperature-dependent magnetic susceptibility of a one-dimensional linear Heisenberg antiferromagnetic chain.

1. Introduction

Peculiar structural phase transitions have been reported involving dramatic changes in electronic and magnetic properties of the crystals of organic π-molecules.[1−3] Notable among these is the neutral−ionic phase transition in tetrathiafulvalene (TTF)−chloranile (CA) crystals.[4] In the (TTF)(CA) crystal, TTF and CA form a charge-transfer complex of $(TTF^{0.3+})(CA^{0.3-})$ with a neutral electronic ground state in ambient conditions. In the crystal, the π-planes of TTF and CA stacked alternately in the order −TTF−CA−TTF−CA− with a uniform π-stack spacing. Lowering of the temperature induces a phase transition associated with the transformation of the electronic ground state to the ionic state of $(TTF^{0.7+})(CA^{0.7-})$, which causes a weak dimerization in the π-stack.[5] The change in the electronic ground state is explained by the compensation between the electrostatic energy, ionization potential (I_p) of TTF, and electron affinity (E_A) of CA molecules.[4] When the electrostatic energy exceeds $I_p - E_A$, the ionic state becomes stable, which results in dramatic responses in physical properties, such as a sharp peak in the dielectric constant, a conductivity increase by 5 orders of magnitude, and the sudden appearance of magnetic spins.[5] The second example is the temperature-induced semiconductor-metal transition of [bis(ethylenedithiolo)−TTF (BEDT−TTF)]$_2Br_{1.3}I_{1.1}Cl_{0.6}$ crystals, in which dipole−dipole interactions of $Br_{1.3}I_{1.1}Cl_{0.6}$ anions were the cause of the phase transition.[6] The anions of this salt were composed of asymmetrical $(Br-I-I)^-$ and $(Br-I-Cl)^-$ trihalide anions, both of which have dipole moments. Thus, anion positions showed thermal fluctuation at high temperature. Upon cooling, the anions froze at specific positions, which completely canceled the net dipole moments of the anion arrangements. The orientational rearrangement of the dipole moments modified the intermolecular interactions of BEDT−TTF molecules, causing the transition of the electrical conducting behavior from metallic to semiconducting.

From the viewpoint of structural modifications in crystals, the supramolecular cation approach is an effective method. By using supramolecular cations composed of inorganic cations and crown ethers, we can control the overall size and shape of cations in crystals.[7−10] In cases where the alkali-metal cation fits into the cavity of the crown ether, planar M^+(crown ether) structures such as $K^+([18]crown\text{-}6)$ and $Rb^+([18]crown\text{-}6)$ have been obtained. Cations much larger than the crown ether cavity typically formed a sandwich-type $M^+(crown\ ether)_2$ structure. The radii of alkali metal cations increase in the order Li^+ (0.68 Å) < Na^+ (0.98 Å) < K^+ (1.33 Å) < Rb^+ (1.49 Å) < Cs^+ (1.65 Å).[11] The cation radius not only determines the size of

* Address correspondence to these authors: Research Institute for Electronic Science, Hokkaido University. E-mail: takuta@imd.es.hokudai.ac.jp and tnaka@imd.es.hokudai.ac.jp. Phone: +81-11-706-2884. Fax: +81-11-706-4972.

† Research Institute for Electronic Science, Hokkaido University.

‡ Graduate School of Environmental Earth Science, Hokkaido University.

§ CREST, Japan Science and Technology Agency.

10.1021/jp055574a CCC: $33.50
Published on Web 02/23/2006

SCHEME 1: $(M^+)([12]crown\text{-}4)_2[Ni(dmit)_2]^-$ Salts ($M^+ = Li^+$, Na^+, K^+, and Rb^+)

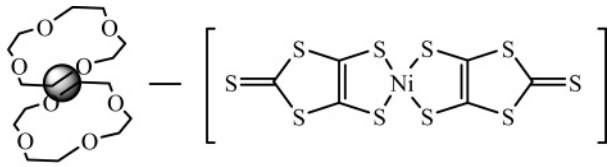

$M^+([12]crown\text{-}4)_2$ $[Ni(dmit)_2]^-$

TABLE 1: Crystal Stoichiometry, Shape, and Space Group of Salts 1−4

entry	stoichiometry[a]	shape	space group
1	$(Li^+)([12]crown\text{-}4)_2[Ni(dmit)_2]^-$	block	$P\bar{1}$
2	$(Na^+)([12]crown\text{-}4)_2[Ni(dmit)_2]^-$	block	*C*2/*m* and *C*2/*c*
3	$(K^+)([12]crown\text{-}4)_2[Ni(dmit)_2]^-$	block	*C*2/*m* and *C*2/*c*
4	$(Rb^+)([12]crown\text{-}4)_2[Ni(dmit)_2]^-$	block	*C*2/*c*

[a] Determined by X-ray crystal structural and elemental analysis.

the M^+(crown ethers)-type molecular assembly, but it also modulates the overall shape of supramolecular cations owing to the difference in coordination environment between M^+ and the oxygen atoms of crown ethers, which, at the same time, changes the conformation of the crown ethers. These supramolecular cation structures were introduced into $[Ni(dmit)_2]^-$-based magnetic crystals ($dmit^{2-}$ = 2-thione-1,3-dithiole-4,5-dithiolate),[7−10] in which the anion $[Ni(dmit)_2]^-$ has one $S = {}^1/_2$ spin. The supramolecular cations of M^+(crown ethers) act as closed-shell countercations in ionic M^+(crown ethers)$[Ni(dmit)_2]^-$ salts. Even by using simple (M^+)(crown ethers) and (M^{2+})(crown ethers)$_2$, a variety of $[Ni(dmit)_2]^-$ crystal arrangements such as monomers, linear one-dimensional Heisenberg chains, two-dimensional Heisenberg chains, dimers, and spin-ladders were obtained, each exhibiting different magnetic properties.[8−10] The lattice energy of magnetic M^+(crown ethers)$[Ni(dmit)_2]^-$ crystals is dominated by electrostatic interactions between M^+(crown ethers) and $[Ni(dmit)_2]^-$, van der Waals and dipole−dipole interactions, etc. Structural modifications in M^+(crown ethers) are expected to modify these interactions, through which we can control the structural phase transitions. Another interesting point is the coupling between structural phase transitions and magnetism. Since the magnitude of the intermolecular interaction between $[Ni(dmit)_2]^-$ anions is directly related to the magnetic exchange energy, structural phase transitions change the magnetic properties of the crystal significantly. In the present study, simple supramolecular cation structures of $M^+([12]crown\text{-}4)_2$ were introduced into the crystals to seek novel phase transitions in magnetic $[Ni(dmit)_2]^-$ salts. An increase in the size of the alkali metal cation from Li^+ to Na^+, K^+, and Rb^+ modified the size and conformation of the resultant supramolecular cation structures. Na^+ and K^+ induced a structural phase transition of $M^+([12]crown\text{-}4)_2[Ni(dmit)_2]^-$.

2. Experimental Section

2.1. Preparation of $[Ni(dmit)_2]^-$ Salts. The precursor monovalent $(n\text{-}Bu_4N^+)[Ni(dmit)_2]^-$ salt was prepared as described in the literature.[12] The crystals of salts **1**−**4** were grown in CH_3CN, using standard mixing and diffusion methods in a vial (∼30 mL) and H-shaped cells (∼50 mL), respectively. The cation sources of $(M^+)(X^-)$, where X = ClO_4, BF_4, and I, were recrystallized from CH_3CN (distilled prior to use). The details of the crystallization procedure are given in the Supporting Information. Table 1 summarizes the crystal stoichiometry, shape, and space group of salts **1**−**4**. The stoichiometry of crystals **1**−**4** was determined by X-ray structural analysis and elemental analysis. **CAUTION!** Perchlorate cation sources can be explosive and should be handled with care and not heated when dry.

2.2. Crystal Structure Determination. Crystallographic data (Table 2) were collected by a Rigaku RAXIS-RAPID diffractometer using Mo Kα (λ = 0.71073 Å) radiation from a graphite monochromator. Structure refinements were made by using the full-matrix least-squares method on F^2. Calculations were performed with SHELXL-97 software packages.[13] Parameters were refined with use of anisotropic temperature factors except for [12]crown-4 of salts **1** and **2** (T = 298 K) and the hydrogen atom. The large thermal parameter of [12]crown-4 in salts **1** and **2** (T = 298 K) prevented the application of anisotropic thermal parameters.

2.3. Magnetic Susceptibility. The temperature-dependent magnetic susceptibility was measured with a Quantum Design MPMS-XL SQUID magnetometer on polycrystalline samples. The sample masses used for SQUID measurements of salts **1**, **2**, **3**, and **4** were 5.50, 13.8, 9.44, and 17.30 mg, respectively, which were packed in measurement strew by using about 30 mg of polymethylpentene wrap (5 × 5 cm^2). The temperature-dependent susceptibility of blank (χ_{blank}) was obtained by 30 mg wrap in strew, which was subtracted from raw data of

TABLE 2: Crystal Data, Data Collection, and Reduction Parameter of the Salts 1−4

	1	**2**	**2**	**3**	**3**	**4**	**4**
chemical formula	$C_{22}H_{32}O_8S_{10}LiNi$	$C_{22}H_{32}O_8S_{10}NaNi$	$C_{22}H_{32}O_8S_{10}NaNi$	$C_{22}H_{32}O_8S_{10}KNi$	$C_{22}H_{32}O_8S_{10}KNi$	$C_{22}H_{32}O_8S_{10}RbNi$	$C_{22}H_{32}O_8S_{10}RbNi$
formula wt	810.73	826.78	826.78	842.89	842.89	889.26	889.26
space group	$P\bar{1}$ (no. 2)	*C*2/*m* (no. 12)	*C*2/*c* (no. 15)	*C*2/*m* (no. 12)	*C*2/*c* (no. 15)	*C*2/*c* (no. 15)	*C*2/*c* (no. 15)
a, Å	12.12(3)	10.48(1)	30.03(4)	10.47(2)	29.87(1)	31.19(5)	30.61 (2)
b, Å	20.95(5)	11.59(2)	11.33(2)	11.58(1)	11.268(6)	11.35(1)	11.144(6)
c, Å	27.35(5)	14.50(2)	10.36(2)	14.49(2)	10.309(5)	10.41(1)	10.275(4)
α, deg	90.92(2)						
β, deg	91.3(2)	92.58(4)	106.47(5)	92.61(4)	106.38(2)	107.04(5)	106.24 (2)
γ, deg	103.6(2)						
V, Å^3	6743(27)	1758(4)	3378(9)	1756(3)	3329(2)	3522(8)	3366(3)
Z	8	2	4	2	4	4	4
D_{calc}, g·cm^{-1}	1.597	1.561	1.625	1.594	1.682	1.677	1.755
T, K	298	298	100	298	100	298	100
μ, cm^{-1}	12.37	11.98	12.48	13.06	13.78	25.55	26.75
no. of measd reflcns	81169	14099	20393	14386	15605	16843	15378
no. of independent reflcns	28994	2093	3788	2104	3812	4018	3826
$R(I=2\sigma)$	0.0995	0.0862	0.0599	0.0423	0.0206	0.0421	0.0338
R(all)	0.2080	0.0965	0.0664	0.0500	0.0248	0.0643	0.0458
GOF	1.065	1.201	1.066	1.105	0.978	0.809	1.051

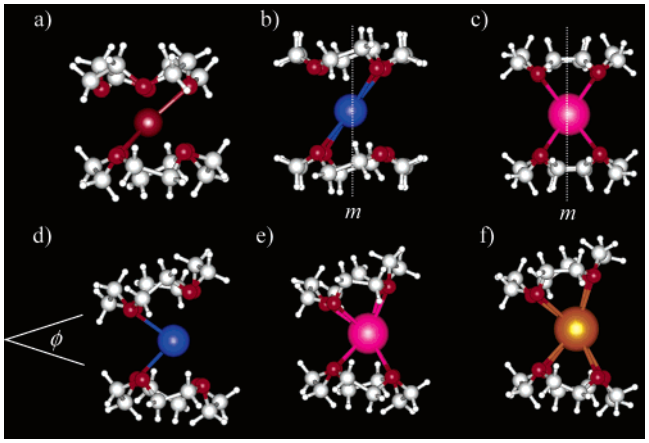

Figure 1. $(M^+)([12]crown\text{-}4)_2$ structures of salts (a) **1**, (b) **2** ($T = 298$ K), (c) **3** ($T = 298$ K), (d) **2** ($T = 100$ K), (e) **3** ($T = 100$ K), and (f) **4** viewed parallel to the mean O4 plane of [12]crown-4. ϕ is the dihedral angle between the two mean O4 planes of [12]crown-4.

temperature-dependent χ_{raw} of salts **1**−**4**. The applied magnetic field was 10000 Oe for all measurements. The diamagentic susceptibilities of salts **1**, **2**, **3**, and **4** were estimated as 2.13, 2.93, 3.79, and 4.02×10^{-4} emu mol^{-1} per $[Ni(dmit)_2]^-$ anion, which were obtained by the fitting of χ_{mol} vs T^{-1} plots.

2.4. Calculation of Dipole Moments and Transfer Integrals. The dipole moments of $M^+([12]crown\text{-}4)_2$ structures ($M^+ = Na^+$, K^+, and Rb^+) were calculated by using the B3LYP/6-31+G(d,p) for salts **2** and **3** and the LANL2DZ basis set for salt **4**.[14a] Atomic coordinates based on the X-ray crystal structural analysis were used for the calculation. The transfer integrals (t) were calculated within the tight-binding approximation, using the extended Hückel molecular orbital method. The LUMO of the $[Ni(dmit)_2]^-$ molecule was used as the basis function.[14b] Semiempirical parameters for Slater-type atomic orbitals were obtained from the literature.[14b] The t values between each pair of molecules were assumed to be proportional to the overlap integral (S) via the equation $t = -10S$ eV.

2.5. Differential Scanning Calorimetry (DSC). Temperature-dependent DSC measurements were carried out on ~10 mg powder samples with a Rigaku Thermo Plus DSC 8230 with an Al_2O_3 reference. The endothermic signals were measured between 110 and 550 K at a scanning rate of 5 K·min^{-1}.

3. Results and Discussion

The same crystal stoichiometry of $M^+([12]crown\text{-}4)_2[Ni(dmit)_2]^-$ ($M^+ = Li^+$, Na^+, K^+, and Rb^+) was observed in salts **1**−**4**. In the crystals, the supramolecular cation assumed a sandwich-type $M^+([12]crown\text{-}4)_2$ structure, in which the M^+ ion was coordinated by eight oxygen atoms of upper and lower [12]crown-4 molecules. Structural phase transition was observed at 222.5 and 270 K in salts **2** and **3**, respectively, as determined by temperature-dependent X-ray crystal structural analysis, DSC, and magnetic susceptibility measurements. The space group of salts **2** and **3** at 298 and 100 K was $C2/m$ and $C2/c$, respectively (Table 2). The molecular arrangements of cations and anions in salts **2** and **3** at 100 K were isomorphous to those of salt **4** at 298 K. The space group of salt **4** was $C2/c$ at 100 and 298 K. We will now discuss the differences in the cation structures, $[Ni(dmit)_2]^-$ arrangements, and temperature-dependent magnetic susceptibilities of salts **1**−**4**.

3.1. Cation Conformations. Figure 1 summarizes the supramolecular cation structures of salts **1**−**4**. The conformational differences between the $(M^+)([12]crown\text{-}4)_2$ structures are represented by the following parameters: average M^+−O distance, dihedral angle between the two O4 planes of [12]-crown-4 (ϕ), and deviation distance of M^+ ion from the mean O4 plane of [12]crown-4 ($d_{M-Oplane}$) (Table 3). Four kinds of $Li^+([12]crown\text{-}4)_2$ units (**A**, **B**, **C**, and **D**) were observed as crystallographically asymmetric units in salt **1**. The dihedral angle ϕ of these units was close, ranging from 1° to 3°, which resulted in an almost parallel arrangement of the two [12]crown-4 planes. Average Li^+−O distances of units **A**, **B**, **C**, and **D** were 2.38, 2.38, 2.38, and 2.36 Å, respectively.

The cation structure in salts **2** and **3** at 298 K ($C2/m$) was constructed from a half unit of crystallographically asymmetric [12]crown-4 because of the mirror plane normal to the molecular plane of [12]crown-4 (Figure 1b,c). The Na^+ in salt **2** and K^+ in salt **3** at 298 K were located on a mirror plane, resulting in a parallel arrangement of the two mean O4 planes of [12]crown-4 ($\phi = 0$). The cation structures of salts **2** and **3** at 298 K do not possess a dipole moment. With the change in crystal symmetry from $C2/m$ ($T = 298$ K) to $C2/c$ ($T = 100$ K) in salts **2** and **3**, the conformation of $Na^+([12]crown\text{-}4)_2$ and $K^+([12]crown\text{-}4)_2$ changed dramatically (Figure 1d,e). The cation structure of salt **4** ($C2/c$) was similar to those of salts **2** and **3** at 100 K. One [12]crown-4 molecule became a crystallographically asymmetric unit in salts **2** ($T = 100$ K), **3** ($T = 100$ K), and **4** ($T = 100$ and 298 K), in which the molecular planes of two [12]crown-4 were related by 2_1-symmetry with $\phi \neq 0$. The ϕ in salts **2** ($T = 100$ K), **3** ($T = 100$ K), and **4** ($T = 100$ K) were 22.6°, 24.1°, and 30.8°, respectively, indicating finite dipole moments (μ). The magnitudes of μ of $Na^+([12]crown\text{-}4)_2$ ($T = 100$ K), $K^+([12]crown\text{-}4)_2$ ($T = 100$ K), and $Rb^+([12]crown\text{-}4)_2$ ($T = 100$ K) based on the atomic coordinates determined by the crystal structural analysis were 0.88, 1.24, and 1.37 D, respectively. Larger ϕ angles generated larger μ values. The deformation of cation structures induced by lowering of the temperature suddenly generated the μ observed in salts **2** and **3**, while the $Rb^+([12]crown\text{-}4)_2$ structure showed a dipole moment at 298 K.

The average Na^+−O distances in salt **2** were almost temperature independent: 2.76 Å ($T = 298$ K) and 2.78 Å ($T = 100$ K). The minimum Na^+−O1 distance of 2.71(1) Å at 298 K was observed at a diagonal position of the an upper and lower [12]crown-4 molecule (Figure 1b), while that of 2.723(4) Å at 100 K was observed to the left-hand side of the upper and lower [12]crown-4 (Figure 1d). The average K^+−O distance of salt **3**

TABLE 3: Structural Parameters of Cation Units for Salts 1−4[a]

		2		**3**		**4**	
	1	$T = 298$ K	$T = 100$ K	$T = 298$ K	$T = 100$ K	$T = 298$ K	$T = 100$ K
M^+-O_{AV}	2.38	2.76	2.78	2.77	2.78	2.97	2.93
$d_{M-Oplane}$	1.37	1.91	1.93	1.93	1.93	2.16	2.12
ϕ	1−3[b]	0	22.6	0	24.1	31.0	30.8
μ[c]	-	0.88	0	0	1.24	1.37	1.37

[a] The parameters $d_{M-Oplane}$ and ϕ are defined in the text. [b] Average values of four kinds of $Li^+([12]crown\text{-}4)_2$ units. [c] Calculated dipole moment of the $M^+([12]crown\text{-}4)_2$ structure, using the basis function of B3LYP/6-31+G(d,p) for salts **2** and **3** and B3LYP/LANL2DZ for salt **4**.

TABLE 4: Transfer Integrals ($t \times 10^{-3}$ eV),[a] Structural Parameters of $[Ni(dmit)_2]^-$, and Magnetic Parameters of Salts 1−4

		2		3		4	
	1	$T = 298$ K	$T = 100$ K	$T = 298$ K	$T = 100$ K	$T = 298$ K	$T = 100$ K
t_1, meV	4.67	7.65	40.0	12.60	46.5	32.8	56.2
t_2, meV	3.85	0.92	−0.65	2.16	0.16	0.52	0.52
t_3, meV	3.32						
t_4, meV	0.35						
φ, deg		0	27.2	0	29.0	26.0	29.4
θ, K	−0.11	−29.6[c]					
J/k_B, K			−30.6	−46.2			−62.4
magnetism[b]	C − W	C − W	1D H. A.	1D H. A.		1	1D H. A.

[a] The transfer integrals (t) were obtained by the LUMO of $[Ni(dmit)_2]^-$ based on the extended Hückel calculation ($t = -10S$ eV, S is overlap integral). [b] 1D H.A. is the one-dimensional linear Heisenberg antiferromagnetic chain and C−W is the Curie−Weiss model. [c] Weiss temperature (θ) was determined by the fit in the temperature range above 220 K.

at 298 K (2.77 Å) was almost the same at 100 K (2.78 Å). The cation structure of $Rb^+([12]crown\text{-}4)_2$ in salt **4** (Figure 1f) was isostructural to that of salts **2** and **3** at 100 K, whose average Rb^+−O distances were 2.97 ($T = 298$ K) and 2.93 Å ($T = 100$ K).

3.2. $[Ni(dmit)_2]^-$ Anion Arrangements. Each $[Ni(dmit)_2]^-$ anion has one $S = {}^1/_2$ spin, and the conformation of $[Ni(dmit)_2]^-$ anions is directly related to the magnetism. Transfer integrals based on the extended Hückel molecular orbital calculations were employed to evaluate the magnitude of the intermolecular interactions between $[Ni(dmit)_2]^-$ anions within the crystals.[15] The overlap integrals (S) between the LUMO of $[Ni(dmit)_2]^-$ were transformed to the transfer integrals (t) from the empirical relation of $t = -10$ S eV.[14b] The effective on-site Coulomb repulsive energy (U_{eff}) in solid was smaller than the bare on-site Coulomb energy (U_{bare}) in solution due to polarization energy of the crystal lattice. Since the crystal structures of salts **2**−**4** were isostructural to each other, the magnitudes of U_{eff} in solid should be similar to each other. Therefore, the magnetic exchange energy (J) is proportional to the square of the transfer integral,

$$J \propto \frac{4t^2}{U_{eff}} \qquad (1)$$

Table 4 summarizes the transfer integrals, dihedral angles of nearest-neighboring $[Ni(dmit)_2]^-$ planes (φ), and magnetic parameters of salts **1**−**4**.

3.3. Zigzag Chain of $[Ni(dmit)_2]^-$ in Salt 1. Salt **1** contained four kinds of crystallographically asymmetric $[Ni(dmit)_2]^-$ anions (**A**−**D**). Parts a and b of Figure 2 show the $[Ni(dmit)_2]^-$ and $Li^+([12]crown\text{-}4)_2$ arrangements, respectively, viewed along the *a* axis. Four kinds of $Li^+([12]crown\text{-}4)_2$ cations formed zigzag chains along the *c* axis. Lateral S−S contacts formed $[Ni(dmit)_2]^-$ dimer pairs of **A**−**A′**, **B**−**B′**, **C**−**C′**, and **D**−**D′** (Figure 2a), where the molecules with the prime symbol were generated by symmetry inversion. The transfer integrals within the **A**−**A′**, **B**−**B′**, **C**−**C′**, and **D**−**D′** dimers were 4.67, 3.85, 3.32, and 0.35 meV, respectively. These values are not sufficient to realize effective intermolecular interactions between $[Ni(dmit)_2]^-$ anions. The **A**−**A′** and **B**−**B′** dimers were found on the zigzag chains of $Li^+([12]crown\text{-}4)_2$ along the *c* axis without effective intermolecular interactions along the *c* axis. The long axes of $[Ni(dmit)_2]^-$ **C** and **D** were almost normal to the π-planes of $[Ni(dmit)_2]^-$ **A** and **B**, penetrating into the spaces between the zigzag chains of **A** and **B** along the *a* axis. The intermolecular interactions between the $[Ni(dmit)_2]^-$ dimers were less than 0.1 meV, suggesting that $[Ni(dmit)_2]^-$ dimers were isolated from each other.

3.4. Temperature-Induced Structural Phase Transition in Salt 2. Structural transformation from the space group *C*2/*m* ($T = 298$ K) into *C*2/*c* ($T = 100$ K) almost doubled the unit cell volume (Table 2). A quarter of the $[Ni(dmit)_2]^-$ were crystallographically asymmetric units at 298 K, while one-half of the $[Ni(dmit)_2]^-$ were symmetric units at 100 K. Figure 3a shows the unit cell of salt **2** at 298 K viewed along the *a* axis. An alternate layer structure between the $[Ni(dmit)_2]^-$ anions and $Na^+([12]crown\text{-}4)_2$ cations in the *ab* planes was observed along the *c* axis, which isolated $[Ni(dmit)_2]^-$ layers along the *c* axis. Within the $[Ni(dmit)_2]^-$ layer, a one-dimensional uniform chain of $[Ni(dmit)_2]^-$ anions was observed along the *a* axis (Figure 3b). The magnitude of the t_1 interaction (7.65 meV at 298 K) was much smaller than that of the lateral t_2 interaction along the *b* axis (0.92 meV). The one-dimensional t_1 interaction along the *a* axis represented the effective intermolecular interaction within the crystal.

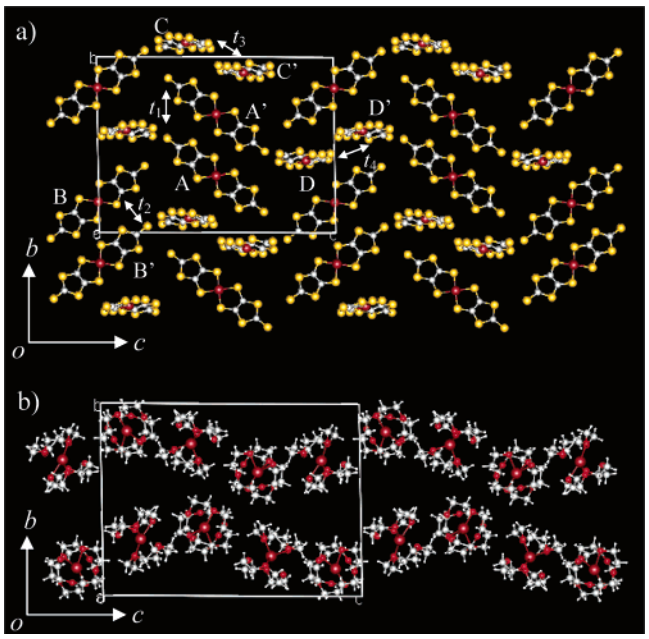

Figure 2. Crystal structures of salt **1**: (a) $[Ni(dmit)_2]^-$ arrangement in the *bc* plane viewed along the *a* axis and (b) $Li^+([12]crown\text{-}4)_2$ cation arrangement in the *bc* plane viewed along the *a* axis.

Figure 3c shows the unit cell of salt **2** ($T = 100$ K) viewed along the *c* axis. After the change in space group from *C*2/*m* to *C*2/*c*, the unit cell parameter $a = 30.03(4)$ Å was almost twice the value of $c = 14.50(2)$ Å ($T = 298$ K). At 100 K, the effective intermolecular interaction in the one-dimensional linear chain of $[Ni(dmit)_2]^-$ anions along the *c* axis was $t_1 = 40.0$ meV, which was about five times larger than the t_1 interaction at 298 K. The interchain t_2 interaction along the *b* axis (0.65 meV) was similar in magnitude to that at 298 K. Parts a and b of Figure 4 illustrate the $[Ni(dmit)_2]^-$ arrangements at 298 and 100

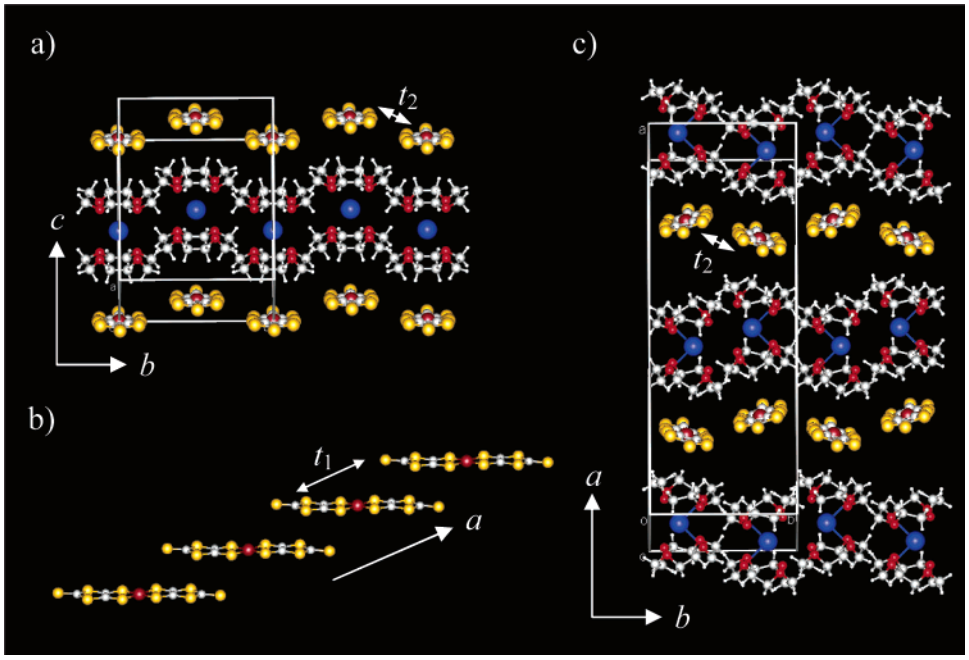

Figure 3. Crystal structures of salt **2**: (a) unit cell viewed along the *a* axis and (b) one-dimensional uniform $[Ni(dmit)_2]^-$ chain along the *a* axis (T = 298 K) and (c) unit cell viewed along the *c* axis (T = 100 K). The intermolecular transfer integrals (t_1 and t_2) are shown.

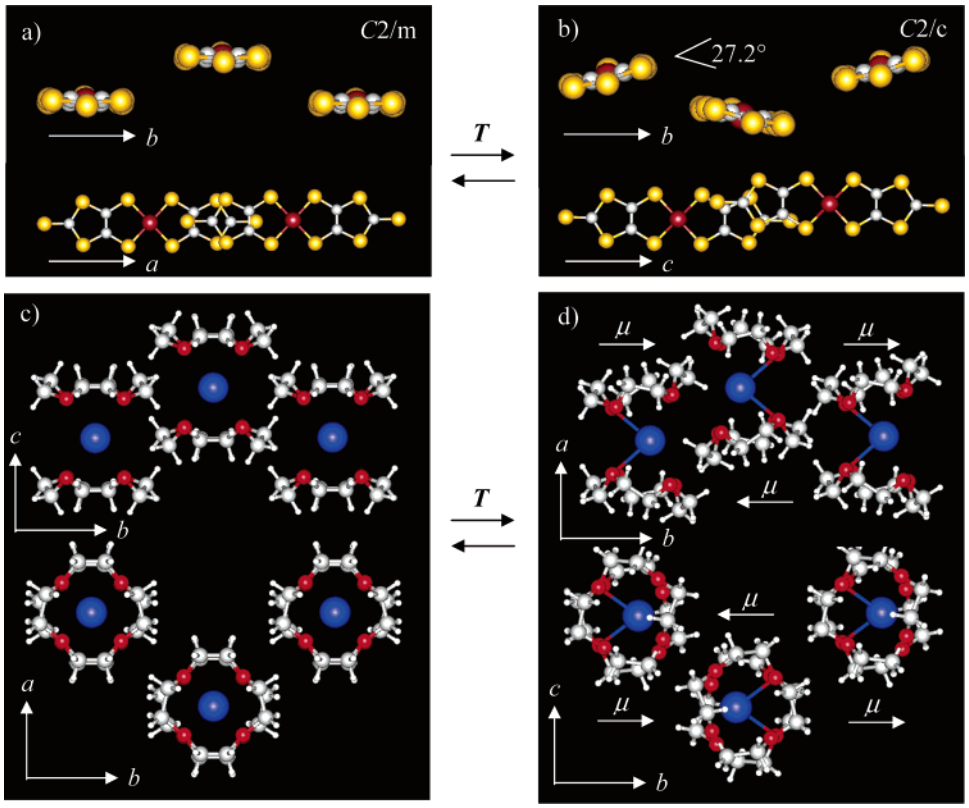

Figure 4. Structural transformation of $[Ni(dmit)_2]^-$ and $Na^+([12]crown\text{-}4)_2$ arrangements in salt **2** induced by lowering of the temperature. $[Ni(dmit)_2]^-$ arrangement viewed along the long axis (upper) and normal to the π-plane of $[Ni(dmit)_2]^-$ (lower) at (a) 298 and (b) 100 K, respectively. Na^+-$([12]crown\text{-}4)_2$ conformation and arrangement viewed parallel (upper) and normal to the mean O4 plane of [12]crown-4 (lower) at (c) 298 and (d) 100 K. The space group *C*2/*m* (T = 298 K) changed to *C*2/*c* (T = 100 K). The dipole moments (μ) of the cation structures (T = 100 K) are schematized.

K viewed along the long axis of $[Ni(dmit)_2]^-$ (upper) and normal to the of π-plane of $[Ni(dmit)_2]^-$ (lower). The parallel arrangement of π-planes of $[Ni(dmit)_2]^-$ molecules (T = 298 K) changed to a twisted arrangement with a dihedral angle of 27.2° (T = 100 K). The $\pi-\pi$ overlapping modes between $[Ni(dmit)_2]^-$ anions differed considerably between high and low temperatures (lower in Figure 4a,b). The π-plane of $[Ni(dmit)_2]^-$ anions slipped mainly along the short axis of $[Ni(dmit)_2]^-$ at 100 K. Such structural transformations of the $[Ni(dmit)_2]^-$ conformation increased the magnitude of the t_1 interaction from 7.65 meV (T = 298 K) to 40.0 meV (T = 100 K).

Parts c and d of Figure 4 show cation conformations and packing arrangements at 298 and 100 K, respectively. Although the cell parameters of a = 10.48(1) Å and b = 11.59(2) Å (T

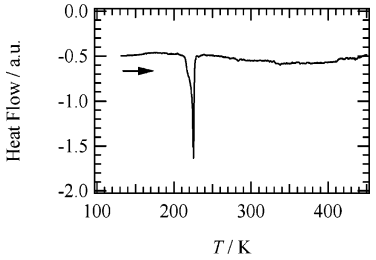

Figure 5. DSC diagram of salt **2** at the heating process from 120 to 450 K.

= 298 K) of salt **2** were reduced to $c = 10.36(2)$Å and $b = 11.32(2)$ Å ($T = 100$ K), respectively, the *a* axis at 100 K was more than twice as large as the *c* axis at 298 K. The conformational change of $Na^+([12]crown\text{-}4)_2$ reduced the overall cation length along the *b* axis, while it increased the cation length along the *a* axis at 100 K. The dihedral angle of the two mean O4 planes of [12]crown-4 in the cation structure of salt **2** ($\phi = 22.6°$ at 100 K) was comparable to that of φ (27.2° at 100 K) for the twisted $[Ni(dmit)_2]^-$ arrangement. The conformational change of the cation structure is connected to the structural rearrangement of $[Ni(dmit)_2]^-$ anions from a parallel ($T = 298$ K) to a twisted arrangement of the π planes ($T = 100$ K), which also increased the thickness of the $[Ni(dmit)_2]^-$ layer along the *a* axis.

The structural phase transition showed up in differential scanning calorimeter (DSC) scans as a sharp endothermic peak at 222.5 K, whose transition enthalpy was 4.71 kJ mol^{-1} (Figure 5). The conformational change of the cation structure from a parallel ($\phi = 0$) to antiparallel ($\phi \neq 0$) arrangement of the two [12]crown-4 planes in $Na^+([12]crown\text{-}4)_2$ generated the μ within the *bc* plane, oriented along the *b* axis. As mentioned previously, the layer structures of cations within the *bc* plane were separated by the $[Ni(dmit)_2]^-$ layers along the *a* axis. The cation arrangement along the *c* axis was generated by the symmetry operation of translation, while the nearest-neighboring cation arrangement along the *c* axis was related through the inversion center. Thus, the net μ of the crystal was canceled along the *c* axis.

For the temperature-induced structural phase transition of salt **2**, the crystal symmetry of the high-temperature phase (*C*2/*m*) was lower than that of the low-temperature *C*2/*c* phase. Since the molecular displacements of cations and anions were confirmed in X-ray crystal structural analyses of salt **2**, the structural phase transition of salt **2** is classified as the atomic displacement type. The structural phase transition of salt **2** was a first-order transition, in which the entropy of high- and low-temperature phases changed discontinuously at the phase transition temperature ($T_c = 222.5$ K). The magnitude of the entropy change (ΔS), which is the driving force for rearrangement of the cations and anions within the crystals, was estimated to be $\Delta S/T_c \sim 21$ J K^{-1} mol^{-1}.

3.5. Crystal Structures of Salts 3 and 4. Salts **3** ($T = 100$ K) and **4** ($T = 100$ and 298 K) were isostructural to salt **2** (*C*2/*c*) at 100 K, while the structure of salt **3** at 298 K (*C*2/*m*) was the same as that of salt **2** at 298 K. The fundamental $[Ni(dmit)_2]^-$ configuration within salts **2**, **3**, and **4** was a one-dimensional liner chain. The magnitude of t_1 interactions at 298 K for salts **2**, **3**, and **4** was 7.68, 12.6, and 32.8 meV, respectively, which was consistent with the increasing cation size from Na^+ to K^+ and Rb^+ in the $M^+([12]crown\text{-}4)_2$ structure. Although the crystal symmetry of salt **4** differed from those of salts **2** and **3** at 298 K, the larger cation increased the t_1 interaction in the one-dimensional linear chain of $[Ni(dmit)_2]^-$ anions, forming a stronger magnetic chain. In salt **3**, the conformational change of the cation structure induced by lowering the temperature generated a dihedral angle ϕ of 24.1° at 100 K, which was similar in magnitude to the $\varphi = 29.0°$ in the twisted $[Ni(dmit)_2]^-$ arrangement at 100 K. The intermolecular interactions of $[Ni(dmit)_2]^-$ increased from $t_1 = 12.6$ at 298 K to $t_1 = 46.5$ at 100 K, while the magnitude of the lateral t_2 interaction decreased from 2.16 to 0.16 meV with lowering of the temperature. Since the $Rb^+([12]crown\text{-}4)_2$ structure in salt **4** was already deformed with a finite angle ϕ of 31.0° at 298 K, a finite dihedral angle of $\varphi = 26.0°$ was observed in the twisted $[Ni(dmit)_2]^-$ arrangement. The magnitude of the t_1 interaction in *C*2/*c* crystals decreased in the order 56.2 meV (salt **4** at 100 K) > 46.8 meV (salt **3** at 100 K) > 40.0 meV (salt **2** at 100 K), which was consistent with the decrease in the magnitude of φ: 29.4° (salt **4** at 100 K) > 29.0° (salt **3** at 100 K) > 27.2° (salt **2** at 100 K).

The temperature-induced structural phase transition of salt **3** was also observed as an endothermic peak in the DSC measurement at 270 K (see Figure S8 in the Supporting Information). This transition was confirmed by X-ray crystal structural analyses at 298 and 100 K. No high-temperature *C*2/*m* phase was identified in salt **4** in the X-ray crystal structural analysis. Since salts **2** ($T = 100$ K) and **3** ($T = 100$ K) were isostructural to each other, the transition mechanism of salt **3** is thought to be identical with that of salt **2**. However, the transition temperature of salt **3** was about 50 K higher than that

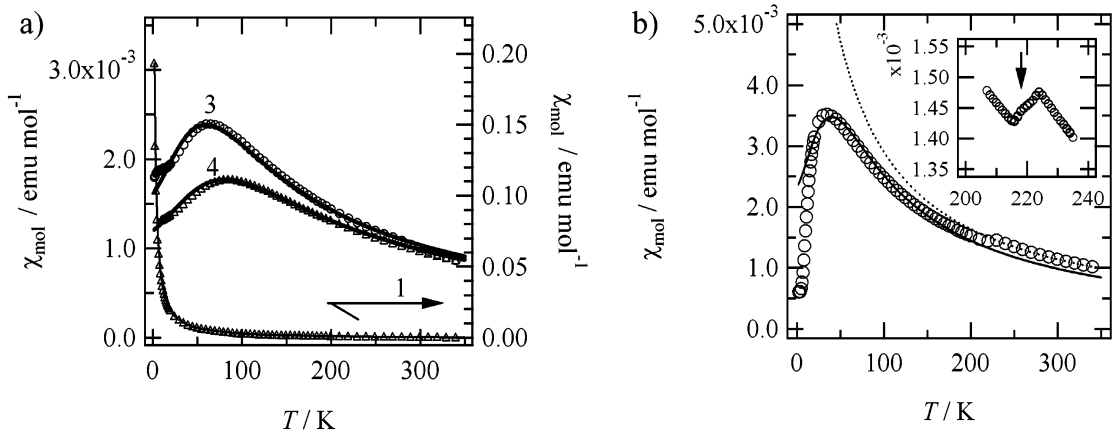

Figure 6. Temperature-dependent magnetic susceptibility of salts **1**, **2**, **3**, and **4**: (a) χ_{mol} vs *T* plots of salts **3** and **4** (left scale) and salt **1** (right scale) per $[Ni(dmit)_2]^-$ anion. (b) χ_{mol} vs *T* plots of salt **2** per $[Ni(dmit)_2]^-$. The inset shows $\chi_{mol}T$ vs *T* plots for the 250−320 K temperature range. The solid and dashed lines represent the fits obtained by using the one-dimensional linear Heisenberg antiferromagnetic model and the Curie−Weiss model, respectively (see text).

of salt **2**. The much larger ion radii of K^+ and Rb^+ compared to that of Na^+ are believed to increase the transition temperature from *C*2/*m* to *C*2/*c*. The calculated μ of the supramolecular cation in salt **3** (1.24 D) was larger than that of salt **2** (0.88 D) at 100 K, which increases the contribution of the dipole−dipole interaction to the crystal lattice energy. Similarly, the μ of the $Rb^+([12]crown\text{-}4)_2$ structure (1.37 D) in salt **4** was larger than those of salts **2** and **3** at 100 K. The much larger deformation in the structurally flexible $M^+([12]crown\text{-}4)_2$ increases the magnitude of the dipole−dipole interaction as part of the crystal lattice energy, which enhanced the transition temperature from the *C*2/*m* to the *C*2/*c* crystal.

3.6. Magnetic Properties of Salts 1−4. Figure 6a shows the temperature-dependent molar magnetic susceptibility (χ_{mol}) per $[Ni(dmit)_2]^-$ anion for salts **1** (right-scale), **3**, and **4** (left-scale). In salt **1**, the weak lateral intermolecular interactions less than ~5 meV were insufficient to yield an effective magnetic exchange interaction between $[Ni(dmit)_2]^-$ anions. The χ_{mol} vs *T* plots for salt **1** obeyed typical Curie−Weiss behavior (C = 0.376 emu K^{-1}) with a Weiss temperature (θ) of −0.1 K, showing a weak antiferromagnetic interaction.[16] The magnetic spins on the $[Ni(dmit)_2]^-$ anion in salt **1** were isolated from each other.

The χ_{mol} vs *T* plots of salts **3** and **4** were similar (left-scale in Figure 6a). Although the structural phase transition was observed at 270 K in salt **3**, no distinct anomaly was observed in the χ_{mol} vs *T* plot around 270 K. The much larger thermal fluctuation of the spin on $[Ni(dmit)_2]^-$ in salt **3** as compared to that of salt **2** prevented a magnetic anomaly from emerging in the χ_{mol} vs *T* plots of salt **3**. A broad maximum in magnetic susceptibility appeared at around 60 and 80 K in salts **3** and **4**, respectively, which is typically observed in one-dimensional linear Heisenberg antiferromagnetic chains and/or isolated dimers.[16a] From the crystal structures, the *t* interactions revealed the presence of one-dimensional linear $[Ni(dmit)_2]^-$ chains. Thus, we applied a one-dimensional linear Heisenberg antiferromagnetic chain model to fit the magnetic susceptibility of salts **3** and **4**.[16b] From the fits of eq 2,

$$\chi_M = \frac{Ng^2{\mu_B}^2}{k_B T}\left(\frac{0.25 + 0.0749\left(\frac{|J|}{k_B T}\right) + 0.0752\left(\frac{|J|}{k_B T}\right)^2}{1 + 0.9931\left(\frac{|J|}{k_B T}\right) + 0.1721\left(\frac{|J|}{k_B T}\right)^2 + 0.7578\left(\frac{|J|}{k_B T}\right)^3}\right) \quad (2)$$

the *J* of salts **3** and **4** was found to be −46.2 and −62.4 K, respectively, at a fixed *C* value of 0.376 emu K^{-1} mol. The ratio of *J*(**3**):*J*(**4**) = 1:1.6 was estimated from eq 1 by using the t_1 values and assuming the same U_{eff} for salts **3** and **4**. This calculated result was almost consistent with the experimental value of *J*(**3**):*J*(**4**) = 1:1.4.

Figure 6b shows the χ_{mol} vs *T* plot of salt **2**. In salt **2**, the crystal structure results indicated that the one-dimensional linear Heisenberg antiferromagnetic chain model would be a reasonable choice. A drop in χ_{mol} was observed at around 230 K due to lowering of the temperature (see the inset of Figure 6b), which was consistent with the first-order structural phase transition temperature observed in the DSC measurement (Figure 5). However, no evident hysteresis was observed in the *T* vs χ_{mol} plot. Below 223 K, the one-dimensional linear Heisenberg antiferromagnetic chain model was applied to explain the χ_{mol} vs *T* behavior of salt **2**. The *J* of −30.6 K with fixed C = 0.376 emu K^{-1} mol was smaller than those of salts **3** (*J* = −46.2 K) and **4** (*J* = −62.4 K). The structural phase transition of salt **2** clearly affected the magnetic susceptibility through the change in *J*. While the low-temperature χ_{mol} vs *T* behavior was fitted by the one-dimensional linear Heisenberg antiferromagnetic chain model, we used the Curie−Weiss model to fit the χ_{mol} vs *T* behavior in the high-temperature range from 223 to 350 K (Figure 6b), which yielded a Weiss temperature of −29.6 K at a fixed *C* of 0.376 emu K mol^{-1}.

4. Summary

Sandwich-type supramolecular cation structures of $(M^+)([12]crown\text{-}4)_2$ (M^+ = Li^+, Na^+, K^+, and Rb^+) were introduced into $[Ni(dmit)_2]^-$-based ionic magnetic crystals with $M^+([12]crown\text{-}4)_2[Ni(dmit)_2]^-$ as the resultant stoichiometry. Two types of supramolecular cation structures were observed: one with a parallel arrangement of the two [12]crown-4 planes, the other with a nonparallel arrangement of the two [12]crown-4 having a dipole moment (μ). Alternating layers of $M^+([12]crown\text{-}4)_2$ cations and $[Ni(dmit)_2]^-$ anions was the fundamental arrangement, in which a one-dimensional linear chain of $[Ni(dmit)_2]^-$ anions was observed with relatively large intermolecular interactions except for the case of $M^+ = Li^+$. The zigzag arrangement of $Li^+([12]crown\text{-}4)_2$ cations induced weak $[Ni(dmit)_2]^-$ dimers through lateral S−S contacts. The magnetic spins of these dimers were isolated from each other (Curie−Weiss behavior). Temperature-dependent magnetic susceptibility of the crystals with *C*2/*c* symmetry (M^+ = Na^+, K^+, and Rb^+) was explained by the one-dimensional linear Heisenberg antiferromagnetic chain model. With increasing temperature, sodium and potassium salts showed a first-order phase transition from the *C*2/*m* to the *C*2/*c* space group at 222.5 ($M^+ = Na^+$) and 270.0 K ($M^+ = K^+$) associated with changes in cation conformations and $[Ni(dmit)_2]^-$ arrangements within the crystal. Upon lowering of the temperature, the structurally flexible supramolecular cations of $M^+([12]crown\text{-}4)_2$ deformed into structures having a dipole moment, which further rearranged to cancel the net μ in the crystals. The atomic displacements in the $[Ni(dmit)_2]^-$ anions and cations occurred simultaneously. The supramolecular cation approach is useful to achieve structural modifications of cation sizes and conformations in the crystals, which gives a phase transition system coupled with magnetic properties. Studies on structural modifications using this approach in magnetic $[Ni(dmit)_2]^-$ salts are currently in progress, aimed at constructing strongly coupled systems of magnetic properties and dynamic motion of cationic structures such as molecular rotations.

Acknowledgment. This work was partly supported by a Grant-in-Aid for Science Research from the Ministry of Education, Culture, Sports, Science, and Technology of Japan. The authors thank Dr. K. Ichimura and Prof. K. Nomura for allowing the use of their SQUID magnetometer.

Supporting Information Available: The preparation condition of salts **1**−**4**, elemental analysis, conditions of X-ray crystal structural analysis, atomic numbering scheme, the DSC scans of salt **3**, and CIF files of crystals **1**−**4**. This material is available free of charge via the Internet at http://pubs.acs.org.

References and Notes

(1) (a) Bernstein, J. *Polymorphism in Molecular Crystals*; Oxford University Press: New York, 2002. (b) Rao, C. N. R. *Acc. Chem. Res.* **1984**, *17*, 83. (c) Bodenheimer, J. S.; Low, W. *Phys. Lett.* **1971**, *36A*, 253. (d) Fujita, W.; Awaga, A. *Science* **1999**, *286*, 261. (e) Itkis, M. E.; Chi, X.; Cordes, A. W.; Haddon, R. C. *Science* **2002**, *296*, 1443. (f) Brusso, J. L.; Clements, O. P.; Haddon, R. C.; Itkis, M. E.; Leitch, A. A.; Oakley, R. T.;

Reed, R. W.; Richardson, J. F. *J. Am. Chem. Soc*. **2004**, *126*, 14692. (g) Avarvari, N.; Faulques, E.; Fourmigué, M. *Inorg. Chem*. **2001**, *40*, 2570.

(2) (a) Katrusiak, A.; Szafrañski, M. *Phys. Rev. Lett*. **1999**, *82*, 576. (b) Akutagawa, T.; Takeda, S.; Hasegawa, T.; Nakamura, T. *J. Am. Chem. Soc*. **2004**, *126*, 291. (c) Beck, B.; Villanueva-Garibay, J. A.; Müller, K.; Roduner, E. *Chem. Mater*. **2003**, *15*, 1739. (d) Szafrañski, M.; Katrusiak, A. *J. Phys. Chem. B* **2004**, *108*, 15709. (e) Nuttall, C. J.; Hayashi, Y.; Yamazaki, K.; Mitani, T.; Iwasa, Y. *Adv. Mater*. **2002**, *14*, 293.

(3) (a) Chollet, M.; Guerin, L.; Uchida, N.; Fukaya, S.; Shimoda, H.; Ishikawa, T.; Matsuda, K.; Hasegawa, T.; Ota, A.; Yamochi, H.; Saito, G.; Tazaki, R.; Adachi, S.; Koshihara, S. *Science* **2005**, *307*, 86. (b) Iwai, S.; Tanaka, S.; Fujinuma, K.; Kishida, H.; Okamoto, H.; Tokura, Y. *Phys. Rev. Lett*. **2002**, *88*, 057402. (c) Okimoto, Y.; Horiuchi, S.; Saitoh, E.; Kumai, R.; Tokura, Y. *Phys. Rev. Lett*. **2001**, *87*, 187401.

(4) (a) Torrance, J. B.; Vazquez, J. E.; Mayerle, J. J.; Lee, V. Y. *Phys. Rev. Lett*. **1981**, *26*, 253. (b) Metzger, R. M.; Torrance, J. B. *J. Am. Chem. Soc*. **1985**, *107*, 117. (c) Takaoka, K.; Kaneko, Y.; Okamoto, H.; Tokura, Y.; Koda, T.; Mitani, T.; Saito, G. *Phys. Rev. B*. **1987**, *36*, 3884.

(5) (a) Cointe, M. Le.; Lemée-Cailleau, M. H.; Cailleau, H.; Toudic, B.; Toupet, L.; Heger, G.; Moussa, F.; Schweiss, P.; Kraft, K. H.; Karl, N. *Phys. Rev. B* **1995**, *51*, 3374. (b) Horiuchi, S.; Okimoto, Y.; Kumai, R.; Tokura, Y. *J. Am. Chem. Soc*. **2001**, *123*, 665. (c) Collet, E.; Cointe, M. B.; Lemée-Cailleau, M. E.; Cailleau, H.; Toupet, L.; Meven, M.; Mattauch, S.; Heger, G.; Karl, N. *Phys. Rev. B* **2001**, *63*, 054105. (d) Okamoto, H.; Mitani, T.; Tokura, Y.; Koshihara, S.; Komatsu, T.; Iwasa, Y.; Koda, T.; Saito, G. *Phys. Rev. B* **1991**, *43*, 8224.

(6) (a) Laukhina, E.; Vidal-Gancedo, J.; Khasanov, S.; Tkacheva, V.; Zorina, L.; Shibaeva, R.; Singleton, J.; Wojciechowski, R.; Ulanski, J.; Laukhin, V.; Veciana, J.; Rovira, C. *Adv. Mater*. **2000**, *12*, 1205. (b) Laukhina, E.; Vidal-Gancedo, J.; Laukin, V.; Veciana, J.; Chuev, I.; Tkachev, V.; Wurst, K.; Rovira, C. *J. Am. Chem. Soc*. **2003**, *125*, 3948.

(7) (a) Nakamura, T.; Akutagawa, T.; Honda, K.; Underhill, A. E.; Coomber, A. T.; Friend, R. H. *Nature* **1998**, *394*, 159. (b) Akutagawa, T.; Hasegawa, T.; Nakamura, T.; Takeda, S.; Inabe, T.; Sugiura, K.; Sakata, Y.; Underhill, A. E. *Chem. Eur. J*. **2001**, *7*, 4902. (c) Akutagawa, T.; Hasegawa, T.; Nakamura, T.; Inabe, T. *J. Am. Chem. Soc*. **2002**, *124*, 8903.

(8) (a) Akutagawa, T.; Nishihara, S.; Takamatsu, N.; Hasegawa, T.; Nakamura, T.; Inabe, T. *J. Phys. Chem. B* **2000**, *104*, 5871. (b) Akutagawa, T.; Hashimoto, A.; Nishihara, S.; Hasegawa, T.; Nakamura, T. *J. Phys. Chem. B*. **2003**, *107*, 66. (c) Nishihara, T.; Akutagawa, T.; Hasegawa, T.; Nakamura, T. *Inorg. Chem*. **2003**, *42*, 2480. (d) Akutagawa, T.; Shitagami, K.; Nishihara, S.; Takeda, S.; Hasegawa, T.; Nakamura, T.; Hosokoshi, Y.; Inoue, K.; Ikeuchi, S.; Miyazaki, Y.; Saito, K. *J. Am. Chem. Soc*. **2005**, *127*, 4397.

(9) (a) Akutagawa, T.; Nakamura, T. *Coord. Chem. Rev*. **2000**, *198*, 297. (b) Akutagawa, T.; Nakamura, T. *Coord. Chem. Rev*. **2002**, *226*, 3.

(10) (a) Nishihara, S.; Akutagawa, T.; Hasegawa, T.; Nakamura, T. *Chem. Commun*. **2002**, 408. (b) Nishihara, S.; Akutagawa, T.; Hasegawa, T.; Fujiyama, H.; Nakamura, T.; Nakamura, T. *J. Solid State Chem*. **2002**, *168*, 661.

(11) *Handbook of Chemistry and Physics*, 83rd ed.; CRC Press: New York, 2002.

(12) Steimecke, G.; Sieler, H. J.; Krimse, R.; Hoyer, E. *Phosphorus Sulfur* **1979**, *7*, 49.

(13) Sheldrick, G. M. University of Götingen, 1993/1997/2001.

(14) (a) Frisch, M. J.; et al. *GAUSSIAN 98*; Gaussian, Inc.: Pittsburgh, PA, 1998. (b) Mori, T.; Kobayashi, A.; Sasaki, Y.; Kobayashi, H.; Saito, G.; Inokuchi, H. *Bull. Chem. Soc. Jpn*. **1984**, *57*, 627.

(15) (a) Scott, J. C. *Semiconductor and Semimetals. High Conducting Quasi-One-Dimensional Organic Crystals*; Conwell, E., Ed.; Academic Press: New York, 1988; p 385. (b) Carlin, R. L. *Magnetochemistry*; Springer-Verlag: Heidelberg, Germany, 1986. (c) Kahn, O. *Molecular Magnetism*; VCH: New York, 1993.

(16) (a) Bonner, J. C.; Fisher, M. E. *Phys. Rev*. **1964**, *135*, A640. (b) Hatfield, E. H.; Estes, W. E.; Marsh, W. E.; Pickens, M. W.; ter Haar, L, W.; Weller, R. R. *Extended Linear Chain Compound*; Miller, J. S., Ed.; Plenum Press: New York, 1983; Vol. 3, p 45.